Automatica 49 (2013) 3023–3031

Contents lists available at ScienceDirect

Automatica

journal homepage: www.elsevier.com/locate/automatica

Fully sensorless robust control of variable-speed wind turbines for efficiency maximization☆

Maria Letizia Corradini [a,1], Gianluca Ippoliti [b], Giuseppe Orlando [b]

[a] Scuola di Scienze e Tecnologie, Università di Camerino, via Madonna delle Carceri, 62032 Camerino (MC), Italy
[b] Dip. di Ingegneria dell'Informazione, Università Politecnica delle Marche, via Brecce Bianche, 60131 Ancona, Italy

ARTICLE INFO

Article history:
Received 21 December 2012
Received in revised form
2 May 2013
Accepted 27 June 2013
Available online 12 August 2013

Keywords:
Wind energy conversion systems
Sensorless control
Maximum power efficiency
Sliding mode control

ABSTRACT

This paper focuses on a sensorless robust power generation control strategy for a variable speed wind energy conversion system based on a permanent magnet synchronous generator. The proposed control strategy combines a robust observer of the aerodynamic torque, a simple technique for extracting rotor position using electrical signals, a robust observer of rotor speed, and a sliding mode based field oriented control strategy. The robust vanishing of the observation errors and tracking error is proved. Reported numerical simulations show that the proposed control policy is effective in terms of efficiency maximization and it is robust with respect to bounded parameter variations affecting the mechanical system.

© 2013 Elsevier Ltd. All rights reserved.

1. Introduction

Among currently available Wind Energy Conversion Systems (WECS), variable-speed Wind Turbines (WTs) are continuously increasing their market share, since they allow us to track changes in wind speed by adapting the shaft speed and thus enable the turbine to operate at its maximum power coefficient over a wide range of wind speeds (Beltran, Ahmed-Ali, & Benbouzid, 2009; Chinchilla, Arnaltes, & Burgos, 2006; Tang, Guo, & Jiang, 2011). As is well known, to achieve the goal of power efficiency maximization, the turbine tip speed ratio should be maintained at its optimum value despite wind variations. Moreover, in order to increase efficiency, the great majority of WECSs belonging to small wind turbine technology are equipped with directly-coupled Permanent Magnet Synchronous Generators (PMSGs) (Robles et al., 2008), which are receiving growing acceptance in industrial applications and energy conversion systems because of their desired features: fast dynamical response, high torque to weight ratio, high efficiency, low noise, and robustness (Mohamed, 2007; Robles et al., 2008; Rossi & Tonielli, 1994; Shyu, Lai, Tsai, & Yang, 2002; Xu & Rahma, 2007; Yang & Zhong, 2007).

The problem of WECS power efficiency maximization has been approached in recent years by different control strategies (for a comprehensive overview of variable speed wind energy conversion systems see Chinchilla et al., 2006, Johnson, Pao, Balas, & Fingersh, 2006, Pao & Johnson, 2011). In particular, the feedback schemes known as Direct Torque Control (Casadei, Profumo, Serra, & Tani, 2002; Zhong, Rahman, Hu, Lim, & Rahman, 1999) and Field Oriented Control (FOC) (Casadei et al., 2002; Murray, Palma, & Husain, 2008) have been largely used. To account for the nonlinear behavior of the electrical and mechanical parts, and to deal with the recognized problem of mechanical parameter variations, different nonlinear and/or robust control techniques have been applied, such as, for instance, gain scheduling (Bianchi, De Battista, & Mantz, 2007), fuzzy logic control (Mohamed, Eskander, & Ghali, 2001), integrator backstepping (Pahlevaninezhad, Eren, Bakhshai, & Jain, 2010), feedback linearization technique (Qiao, Qu, & Harley, 2009) and neural networks based control (Cadenas & Rivera, 2009; Lopez, Velo, & Maseda, 2008). In the framework of robust control techniques, methods based on Sliding Mode control (SM) (Beltran et al., 2009; Chen & Lin, 2011; Ferreira, Bejarano, & Fridman, 2011; Lee, Joo, Back, & Seo, 2010; Valenciaga & Puleston, 2008; Wang & Qin, 2010) have been largely used, since are computational simpler than other robust control approaches.

All the cited control algorithms do require, as well known, feedback information about rotor position and, for wind power transfer optimization, of rotor speed and wind speed. Nevertheless, position or speed sensors of wind turbines equipped with PMSGs are usually physically inaccessible, particularly for large size devices, and the associated circuitry may be poorly reliable. It

☆ The material in this paper was not presented at any conference. This paper was recommended for publication in revised form by Associate Editor Peng Shi under the direction of Editor Toshiharu Sugie.

E-mail addresses: letizia.corradini@unicam.it (M.L. Corradini), gianluca.ippoliti@univpm.it (G. Ippoliti), giuseppe.orlando@univpm.it (G. Orlando).

[1] Tel.: +39 0737 402568; fax: +39 0737 402561.

0005-1098/$ – see front matter © 2013 Elsevier Ltd. All rights reserved.
http://dx.doi.org/10.1016/j.automatica.2013.07.028

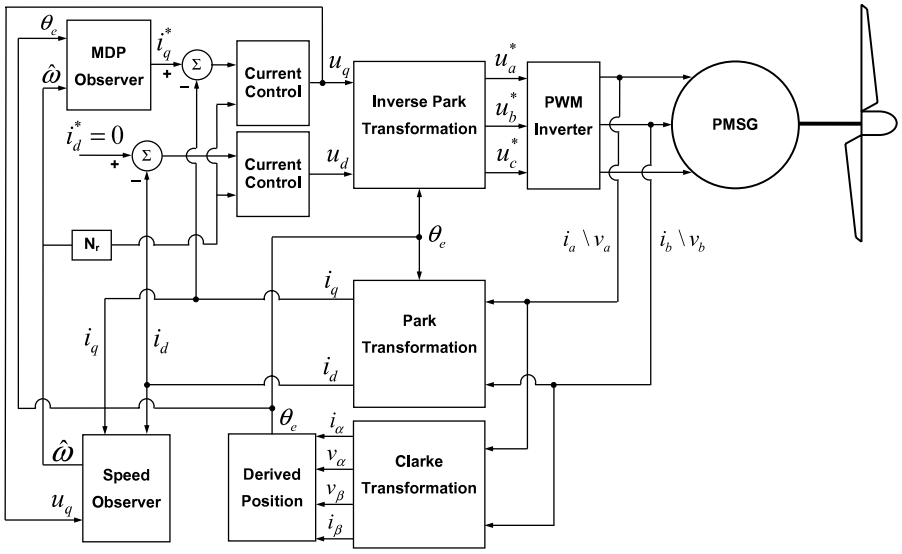

Fig. 1. Field oriented control scheme.

follows that WECS performances in terms of energy transfer, and ultimately cost of energy, may be affected by sensors inaccuracies and/or faults, though extra costs added by rotational transducers are rather limited. For these reasons, the so-called *sensorless control* attracted the industrial interest, and induced an intensive research activity in the control community. Indeed, a number of contributions on this topic have recently appeared for different types of electrical machines. With specific reference to PMSGs (Ortega, Praly, Astolfi, Lee, & Nam, 2011), classification of sensorless techniques is done according to three main threads: motion electromagnetic force (EMF) based, inductance based and flux linkage based (see Acarnley & Watson, 2006 for a review). Depending on the chosen approach, information about rotor position is extracted from high frequency components of the electrical variables, or from their principal components. Adaptive sliding mode observers have been also proposed (Chen, Tomita, Doki, & Okuma, 2000), and extended Kalman filtering has been applied to estimate the whole state vector (Bolognani, Tubiana, & Zigliotto, 2003). As argued in Lee, Hong et al. (2010); Ortega et al. (2011), back-EMF-based methods are largely used in practice, but perform poorly at low-speed regimes and are sensitive to parameter uncertainty. Such behavior can be attributed to the approximations inherently introduced in the linearization of the model of the PMSM, which is highly nonlinear and belongs to a class of plants not addressable by standard nonlinear control techniques. Very recently (Corradini, Ippoliti, & Orlando, 2013), the tracking problem of the Maximum Delivered Power (MDP) characteristic has been solved using the FOC architecture reported in Fig. 1 with the aid of a sliding mode-based robust observer of the aerodynamic torque, but at the price of the availability of rotor speed measurements extracted from encoders.

The key contribution of the present paper is to provide a complete and novel *robust sensorless control scheme* ensuring the achievement of maximum power efficiency of the WECS, not requiring feedback information about rotor speed and position, and about wind velocity. The description of the control strategy is supported by a detailed theoretical development proving closed-loop convergence of observers and the achievement of the control objective in a finite time. A careful simulation study is reported showing the effectiveness of the control scheme. To summarize, the proposed sensorless control strategy for WECS allows us:

- to extract rotor position using electrical signals and an observer of electrical variables;
- to achieve an exact estimate of the rotor velocity within a finite time;
- to achieve the condition on maximum power efficiency of the controlled WECS;
- to avoid the need of wind measurements;
- to account for bounded parameter variations affecting the mechanical system.

The paper is organized as follows. The WECS dynamics are presented in Section 2. In Section 3 some preliminaries are given, and details on the considered controller/observers are discussed. Results on numerical tests are reported in Section 4. The paper ends with comments about the proposed control policy.

2. WECS dynamics

The system model here reported is inspired by the studies (Bianchi et al., 2007; Zaragoza et al., 2011) and references therein. As is well known, wind energy is transformed first into mechanical energy through the WT blades and, ultimately, into electrical energy through the generator.

2.1. Power extraction by a WECS

The aerodynamic (mechanical) power that the wind turbine extracts from the wind is expressed by the following equation (Bianchi et al., 2007):

$$P_a = \frac{1}{2}\rho\pi r^2 C_p(\lambda, \beta) V^3 \tag{1}$$

where ρ is the air density, r is the wind turbine rotor radius, V is the wind speed and the power coefficient $C_p(\lambda, \beta)$ represents the turbine efficiency to convert the kinetic energy of the wind into mechanical energy (Bianchi et al., 2007). This coefficient is a function of both the blade pitch angle β and the tip speed ratio λ which is defined as Qiao et al. (2009):

$$\lambda = \frac{\omega_r r}{V} \tag{2}$$

where ω_r is the WT angular shaft speed. The introduction of the expression of λ in Eq. (1) gives:

$$P_a = \frac{\rho\pi r^3 C_p(\lambda, \beta) V^2}{2\lambda} \cdot \omega_r. \tag{3}$$

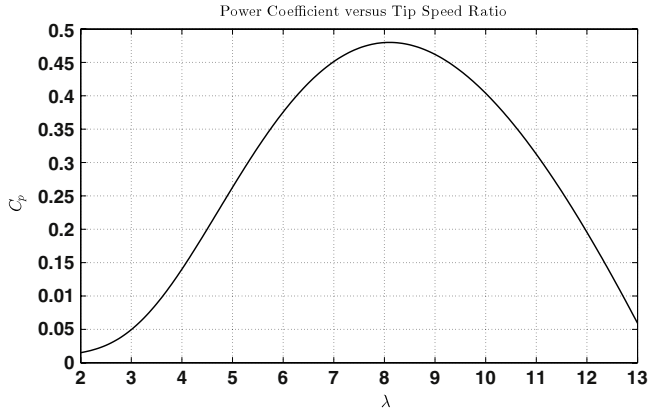

Fig. 2. Power Coefficient C_p. The optimal value is 0.48, for $\lambda = 8.1$.

As a consequence, the torque that the wind turbine extracts from the wind is given by:

$$T_a = \frac{P_a}{\omega_r} = \frac{\rho \pi r^3 C_p(\lambda, \beta) V^2}{2\lambda}. \tag{4}$$

The power coefficient $C_p(\lambda, \beta)$ is a nonlinear function (Monroy & Alvarez-Icaza, 2006; Siegfried, 1998), and depends on blade aerodynamic design and WT operating conditions. In Zaragoza et al. (2011), the following equation is proposed to approximate the power coefficient for a constant value of $\beta = 0°$:

$$C_p(\lambda) = c_1\left(\frac{c_2}{\lambda_1} - c_4\right)e^{-\frac{c_5}{\lambda_1}} + c_6\lambda; \qquad \frac{1}{\lambda_1} = \left(\frac{1}{\lambda} - 0.035\right).$$

The coefficients c_1 through c_6 depend on the shape of the blade and its aerodynamic performance (Beltran et al., 2009; Inc. Princeton Satellite Systems, 2011; Zaragoza et al., 2011).

Fig. 2 shows $C_p(\lambda)$ using the following coefficient values considered in this work: $c_1 = 0.5176$, $c_2 = 116$, $c_4 = 5$, $c_5 = 21$, $c_6 = 0.0068$ (Zaragoza et al., 2011).

Remark 1. Inherent physical limitations of real WECS imply that the wind velocity range that a turbine can face is bounded. It follows that maximum admissible values exist for both the aerodynamic power and the torque which can be extracted by the wind.

2.2. Variable speed and fixed pitch WT regime

The extraction of wind power by a WECS can be divided into different operating regions associated with wind speed, maximum allowable rotor speed and rated power (Beltran et al., 2009). In practice, variable-speed wind turbines have three main regions of operation with respect to wind speed (Johnson et al., 2006). A stopped turbine or a turbine that is just starting up is considered to be operating in region 1. Region 2 is an operational mode with the objective of maximizing wind energy capture. In region 3, which encompasses high wind speeds, the turbine must limit the captured wind power so that safe electrical and mechanical loads are not exceeded. Control of blade pitch is typically used to limit power and speed for turbines operating in region 3, while generator torque control is usually used in region 2. Generator torque, and blade pitch strategies can all be used to shed excess power and limit the turbines energy capture in region 3 but it is common to use only generator torque in region 2, keeping the blade pitch constant at an optimal value for peak energy extraction.

In this paper, a generator torque control with constant blade pitch to maximize energy capture of a variable-speed wind turbine operating in region 2 is considered (Bianchi et al., 2007). This control strategy is commonly used in commercial WTs, especially when operating under low and medium wind speeds, and the control objective is to achieve the maximum power coefficient $C_{p\max}$ regardless of the wind speed. In particular, considering Fig. 2 and the definition of λ in Eq. (2), at any wind speed within the operating range, there is a unique wind-turbine shaft rotational speed to achieve the maximum power coefficient $C_{p\max}$. From Eq. (1), when C_p is controlled at the maximum value, maximum mechanical power is extracted from the wind energy.

In this work the WT operates with a constant pitch angle $\beta = 0°$ and from Fig. 2 the maximum power coefficient $C_{p\max} = 0.48$ is achieved for a tip speed ratio value $\lambda_{\text{opt}} = 8.1$. Thus, the optimal WT angular shaft speed is given by:

$$\omega_{ro} = \frac{\lambda_{\text{opt}} V}{r}. \tag{5}$$

2.3. PMSG modeling

In the (α, β) reference frame, the electrical equations of a PMSG can be written as:

$$\begin{cases} \dfrac{di_\alpha(t)}{dt} = -\dfrac{R}{L}i_\alpha(t) + \omega\dfrac{\lambda_0}{L}\sin(\theta_e(t)) + \dfrac{1}{L}v_\alpha(t) \\ \dfrac{di_\beta(t)}{dt} = -\dfrac{R}{L}i_\beta(t) - \omega\dfrac{\lambda_0}{L}\cos(\theta_e(t)) + \dfrac{1}{L}v_\beta(t) \end{cases} \tag{6}$$

where $i_\alpha(t)$ and $i_\beta(t)$ are the stator currents; $v_\alpha(t)$ and $v_\beta(t)$ are the stator voltages; R is the winding resistance and L is the winding inductance, λ_0 is the flux linkage of the permanent magnet, θ_e and ω are the electrical angular position and speed, respectively, of the generator rotor.

The electrical torque T_e is given by:

$$T_e(t) = K_t(i_\beta(t)\cos(\theta_e(t)) - i_\alpha(t)\sin(\theta_e(t))) \tag{7}$$

in which $K_t = \frac{3}{2}\lambda_0 N_r$ is the torque constant with N_r the number of pole pairs.

Denoting the mechanical angular position and speed of the rotor by θ_r and ω_r, respectively, the following relation holds:

$$N_r = \frac{\omega_e}{\omega_r} = \frac{\theta_e}{\theta_r}. \tag{8}$$

In the following it will be assumed that $N_r = 1$, therefore $\omega_e = \omega_r = \omega$ and $\theta_e = \theta_r$.

The mechanical motion equation is described by:

$$J\dot{\omega}_r(t) + K\omega_r(t) + B\theta_r(t) = T_a(t) - T_e(t) \tag{9}$$

$$\dot{\theta}_r(t) = \omega_r(t) \tag{10}$$

where J is the total mechanical inertia of the PMSG and K and B are the coefficient of viscous friction and stiffness, respectively. The torque $T_a(t)$ summarizes the effect of the aerodynamic torque (generally known with large inaccuracy) and $T_e(t)$ is the generator electromagnetic torque. The coefficients appearing in the PMSG mechanical model are assumed affected by unknown but bounded uncertainties:

Assumption 2.1. The model parameters B and K appearing in (9) are uncertain, with bounded uncertainty:

$$B = \bar{B} + \Delta B; \qquad K = \bar{K} + \Delta K;$$
$$|\Delta B| \le \rho_B; \qquad |\Delta K| \le \rho_K;$$

ρ_B, ρ_K being bounding known positive constants.

Remark 2. The inertia parameter J has been assumed known only for simplifying the statement of the next results. As it will be clear in the following, a bounded variation for this parameter can be accounted for with straightforward changes.

3. Sensorless control design

The control strategy proposed here consists of the following modules:

- a subsystem able to exactly derive rotor position from generator currents, and used for performing the Park transformation (Rotor Position Derivation Subsystem);

- a novel robust observer of rotor speed using currents measurements (Rotor Speed Observer Subsystem);
- a novel robust estimator of the aerodynamic torque T_a (Aerodynamic Torque Observer Subsystem);
- a robust observer-based controller designed in order to impose that the required electrical torque T_e robustly achieves power efficiency maximization (i.e. designed such that the robust tracking of the optimum aerodynamic torque is guaranteed for a suitable choice of the control variable T_e) by setting a suitable reference current $i_q^*(t)$ in the framework of the FOC strategy of Fig. 1 (Control Module).

Closed loop convergence of the whole control scheme will be theoretically proved in the following. A detailed description of each subsystem is reported below, along with the pertinent technical developments. Pros of the control strategy here proposed can be summarized in:

- avoiding the need of accurate wind measurements, and consequent potential loss of control authority coming from eventual failures affecting anemometers,
- avoiding the need of accurate rotor position and speed measurements, and consequent potential loss of control authority coming from eventual failures affecting encoders,
- avoiding the need of sensors maintenance, being transducers usually physically poorly accessible.

3.1. The control objective: power efficiency maximization

The main control objective to be achieved by the wind turbine, operating in low and medium wind speed conditions, is power efficiency maximization (Bianchi et al., 2007; El-Mokadem, Courtecuisse, Saudemont, Robyns, & Deuse, 2009). To achieve this goal the turbine tip speed ratio should be maintained at its optimum value, λ_{opt}, for different wind speed values. Thus, to extract the maximum available wind power, the generator torque should be designed to follow the optimal torque calculated using the wind speed (to be measured). In other words, the generated power must follow the Maximum Delivered Power (MDP) characteristic for different wind speeds.

Conventional techniques of turbine torque control scheme use wind speed measurements to determine the PMSG reference torque (Fernandez, Mantz, & Battaitotto, 2003), but this technique has some significant drawbacks (Beltran et al., 2009; Bianchi et al., 2007). In fact, the effectiveness of this standard control relies on the accuracy of wind measurements, and is sensitive to any fault which could affect anemometers. Moreover, the derivation of the captured torque is made by means of (9) neglecting the term $J\dot{\omega}_r + K\omega_r + B\theta_r$, which is not realistic in many cases. Finally, reliable measurements of rotor angular position and speed are needed. Though extra costs added by rotational transducers are rather limited, the associated circuitry may be poorly reliable or, more importantly, their installation and maintenance are usually physically inaccessible, particularly for large size devices.

To overcome the discussed oversimplifications, a modified version of the torque control scheme is here used, consisting in tracking the $C_{p\max}$ locus in the low and medium wind speed region (Bianchi et al., 2007; El-Mokadem et al., 2009) where the turbine has to operate at the peak of its C_p curve. It is worth noting that, in the standard version of the control scheme, the measured turbine speed ω_r is used to determine the optimum aerodynamic torque, deduced from Eqs. (2) and (4) in MDP mode:

$$T_{\text{opt}} = \frac{1}{2}\frac{\rho\pi r^5 C_{p\max}}{\lambda_{\text{opt}}^3}\omega_r^2 = k_o\omega_r^2 \tag{11}$$

this T_{opt} being imposed as the PMSG reference torque T_e^* (Johnson et al., 2006; Pao & Johnson, 2011) under the unrealistic assumption that the dynamical behavior of the WECS is neglectable. On the contrary, in the proposed sensorless control strategy, the tracking of the optimum aerodynamic torque is achieved without either speed and wind measurements and without the discussed oversimplifications.

3.2. The rotor position derivation subsystem

This module is aimed at providing the rotor angular position deriving it from measurements of the phase currents $i_a(t)$ and $i_b(t)$, transformed by the Clarke coordinate transformation into the stator coordinate frame (α, β) components, $i_\alpha(t)$ and $i_\beta(t)$ (see Fig. 1). In standard generators, rotor position is given by encoder measurements, and rotor speed is usually estimated as the incremental ratio of encoder positions over one sampling period. Both measurements are therefore highly sensitive to inaccuracies of faults which could affect sensors.

For deriving the rotor angular position θ_r, consider the following observer:

$$\begin{cases} \dfrac{d\hat{i}_\alpha(t)}{dt} = -\dfrac{R}{L}i_\alpha(t) + \dfrac{1}{L}v_\alpha(t) \\ \dfrac{d\hat{i}_\beta(t)}{dt} = -\dfrac{R}{L}i_\beta(t) + \dfrac{1}{L}v_\beta(t) \end{cases} \tag{12}$$

and define the observation errors:

$$e_\alpha(t) = i_\alpha(t) - \hat{i}_\alpha(t); \qquad e_\beta(t) = i_\beta(t) - \hat{i}_\beta(t).$$

The following result can be proved:

Lemma 3. *With reference to the plant (6), under the assumption that the rotor initial position $\theta_r(t)$ at $t = 0$ is available, the angular position θ_e can be derived from currents as follows*

$$\theta_e(t) = \arctan\frac{-e_\beta(t) + \frac{\lambda_0}{L}\sin(\theta_e(0))}{-e_\alpha(t) + \frac{\lambda_0}{L}\cos(\theta_e(0))}. \tag{13}$$

Proof. The dynamics of the observation errors are

$$\dot{e}_\alpha(t) = \frac{\lambda_0}{L}\omega\sin(\theta_e(t)) \tag{14}$$

$$\dot{e}_\beta(t) = -\frac{\lambda_0}{L}\omega\cos(\theta_e(t)) \tag{15}$$

which provides, by integration:

$$e_\alpha(t) = e_\alpha(0) - \frac{\lambda_0}{L}\left[\cos(\theta_e(t)) - \cos(\theta_e(0))\right] \tag{16}$$

$$e_\beta(t) = e_\beta(0) - \frac{\lambda_0}{L}\left[\sin(\theta_e(t)) - \sin(\theta_e(0))\right]. \tag{17}$$

Since the initial condition of the observer (28) can be set equal to the initial value of the (measured) currents, the statement directly follows. ■

Using the (exactly derived) generator rotor position θ_r (see Eq. (13)), the measured phase currents, $i_a(t)$ and $i_b(t)$, can be transformed, by the Park coordinate transformation, into the rotor frame direct and quadrature components, $i_d(t)$ and $i_q(t)$. The following well known model for the electrical equations of a PMSG is obtained:

$$\frac{di_d(t)}{dt} = -\frac{R}{L}i_d(t) + \omega_e(t)i_q(t) + \frac{1}{L}u_d(t) \tag{18}$$

$$\frac{di_q(t)}{dt} = -\frac{R}{L}i_q(t) - \omega_e(t)i_d(t) - \frac{\lambda_0}{L}\omega_e(t) + \frac{1}{L}u_q(t) \tag{19}$$

where (18)–(19) are the electrical equations in the (d, q) reference frame, synchronously rotating with the generator rotor (Zaragoza et al., 2011). In the electrical equations, $i_d(t) = i_\alpha(t)\cos(\theta_e(t))$

$+ i_\beta(t)\sin(\theta_e(t))$ and $i_q(t) = i_\beta(t)\cos(\theta_e(t)) - i_\alpha(t)\sin(\theta_e(t))$ are the d-axis and q-axis stator currents, respectively; $u_d(t)$ and $u_q(t)$ are the d-axis and q-axis stator voltages, respectively. The electrical torque $T_e(t)$ is now given by:

$$T_e(t) = K_t i_q(t). \tag{20}$$

In view of the inherent physical limitations of the real device, the following assumption is introduced:

Assumption 3.1. Bounds exist and are available on the maximum achievable rotor velocity: $-\omega^M \le \omega_r \le \omega^M$ and acceleration: $-\dot\omega^M \le \dot\omega_r \le \dot\omega^M$.

3.3. The rotor speed observer subsystem

This module consists of a robust observer of the rotor angular speed, in the presence of bounded uncertainties affecting the coefficients of the mechanical model of the WECS, largely inaccurate, and without a direct measurement of the rotor position. It is proved that the estimated rotor angular velocity provided by this subsystem converges to the true value after an arbitrary finite time.

Lemma 4. *With reference to the plant (18)–(19), define the following dynamical system:*

$$\dot z(t) = -\frac{R}{L} i_q(t) + \frac{1}{L} u_q(t) + \nu(t) \tag{21}$$

with

$$\nu(t) = \gamma_\nu \left(\omega^M \left(|i_d(t)| + \frac{\lambda_0}{L} \right) + \eta_\nu \right) \operatorname{sign}(e(t)) \tag{22}$$

where $e(t) = i_q(t) - z(t)$, and $\gamma_\nu \ge 1$, $\eta_\nu > 0$ are arbitrary constants. The following observed value $\hat\omega(t)$ of the angular speed $\omega(t)$

$$\hat\omega(t) = -\frac{\nu(t)}{i_d(t) + \frac{\lambda_0}{L}}; \quad i_d(t) \neq -\frac{\lambda_0}{L} \tag{23}$$

converges to the true value $\omega(t)$ in an arbitrary finite time t_f.

Proof. The dynamics of the error $e(t)$ are

$$\dot e(t) = -\omega(t) \left(i_d(t) + \frac{\lambda_0}{L} \right) - \nu(t). \tag{24}$$

Consider the sliding surface $e(t) = 0$. By the imposition of the condition $e(t)\dot e(t) < -\eta_\nu |e(t)|$ in the worst case, the expression of $\nu(t)$ (22) immediately follows. Once the sliding motion has been established (after a finite time depending on η_ν), it holds $e(t) = i_q(t) - z(t) = 0$, and consequently $\dot i_q(t) - \dot z(t) = 0$, therefore it holds $\nu(t) = -\omega(t)\left(i_d(t) + \frac{\lambda_0}{L}\right)$. It follows that $\omega(t) = \hat\omega(t)$ after a finite time t_f arbitrarily set by selecting η_ν. ■

3.4. The aerodynamic torque observer subsystem

This module consists of a robust observer of the aerodynamic torque, able to ensure the tracking $T_a = T_{\text{opt}}$ (11), in the presence of bounded uncertainties affecting the coefficients of the mechanical model of the WECS, largely inaccurate, and without a direct measurement of the rotor speed and position. In other words, this subsystem provides as output the value of T_e (and correspondingly of the reference q-axis current), such that the peak of the C_p curve is tracked. Define the following variables

$$\eta(t) = \int_0^t T_a(\tau)d\tau; \tag{25}$$

$$\eta_{\text{opt}}(t) = \int_0^t k_o \omega_r^2(\tau)d\tau = \int_0^t T_{\text{opt}}(\tau)d\tau; \tag{26}$$

$$\hat\eta_{\text{opt}}(t) = \int_0^t k_o \hat\omega^2(\tau)d\tau \tag{27}$$

and consider the following observer:

$$\dot{\hat\eta}(t) = \bar K \hat\omega(t) + T_e(t) \tag{28}$$

where $\hat\eta(t)$ is the estimate of the variable $\eta(t)$. The following result can be proved:

Theorem 3.1. *The observer (28) is able to guarantee the robust vanishing of the error variables $\eta(t) - \eta_{\text{opt}}(t)$ and $\eta(t) - \hat\eta(t)$, $t > t_f$, for a suitable choice of the control variable $T_e(t)$.*

Proof. Consider the following Lyapunov function

$$W(t) = |\eta_{\text{opt}}(t) - \hat\eta_{\text{opt}}(t)| + |\hat\eta_{\text{opt}}(t) - \hat\eta(t)| + |\eta(t) - \hat\eta(t)| + e^2(t).$$

Proving that the derivative $\dot W(t)$ can be made negative for $t > t_f$ by a suitable choice of $T_e(t)$ ensures that for the closed loop system it holds both $\eta(t) = \hat\eta(t) = \hat\eta_{\text{opt}}(t) = \eta_{\text{opt}}(t)$ and $T_a(t) = T_{\text{opt}}(t)$ (i.e. the control objective is achieved). Since for $t > t_f$ it holds:

$$\begin{aligned}
\dot W(t) &= k_o(\omega^2(t) - \hat\omega^2(t))\operatorname{sign}(\eta_{\text{opt}}(t) - \hat\eta_{\text{opt}}(t)) \\
&\quad + \left(k_o\hat\omega^2(t) - \bar K\hat\omega(t) - T_e(t)\right)\operatorname{sign}(\hat\eta_{\text{opt}}(t) - \hat\eta(t)) \\
&\quad + \left(J\dot\omega(t) + (\bar K + \Delta K)(\omega(t) - \hat\omega(t)) \right. \\
&\quad \left. + (\bar B + \Delta B)\theta_e(t)\right)\operatorname{sign}(\eta - \hat\eta) + e(t)\dot e(t) \\
&\le k_o((\omega^M)^2 + \hat\omega^2(t)) - T_e^{(n)}(t)\operatorname{sign}(\hat\eta_{\text{opt}}(t) - \hat\eta(t)) \\
&\quad + J\dot\omega^M + (\bar K + \rho_K)(\omega^M + |\hat\omega(t)|) \\
&\quad + J\dot\omega^M + (\bar B + \rho_B)|\theta_e(t)|
\end{aligned} \tag{29}$$

having designed

$$T_e(t) = -\bar K\hat\omega(t) + k_o\hat\omega^2(t) + T_e^{(n)}(t)$$

and having taken the worst case condition under Assumptions 2.1–3.1, recalling that $\omega(t) = \hat\omega(t)$ for $t > t_f$ in view of Lemma 4. To impose that $\dot W(t) < -\eta_\omega$ for a predefined positive constant $\eta_\omega > 0$, it is enough to choose $T_e^{(n)}(t)$ as follows:

$$\begin{aligned}
T_e^{(n)}(t) &= \gamma_\omega \left[\rho_\omega(t) + k_o((\omega^M)^2 \right. \\
&\quad \left. + \hat\omega^2(t)) + \eta_\omega\right]\operatorname{sign}(\eta_{\text{opt}} - \hat\eta)
\end{aligned} \tag{30}$$

with

$$\rho_\omega(t) = \left[J\dot\omega^M + (\bar K + \rho_K)(\omega^M + |\hat\omega(t)|) + (\bar B + \rho_B)|\theta_e(t)|\right]$$

with $\gamma_\omega \ge 1$. ■

Remark 5. The previous result ensures that $T_a(t) = T_{\text{opt}}(t)$ for $t > t_f$, hence it follows immediately that setting a reference current

$$i_q^*(t) = \frac{1}{K_t}\left(-\bar K\hat\omega(t) + T_e^n(t) + k_o\hat\omega^2(t)\right) \tag{31}$$

the condition of maximum energy conversion is achieved for $t > t_f$. Moreover, the derivative $\frac{di_q^*(t)}{dt}$ is always well defined and bounded for $t > t_f$:

$$\left|\frac{di_q^*(t)}{dt}\right| \le \frac{1}{K_t}\left((\bar K + 2k_o|\hat\omega(t)|)|\dot{\hat\omega}(t)| + \left|\frac{dT_e^n(t)}{dt}\right|\right) \quad t > t_f. \tag{32}$$

3.5. The control module

In order to ensure the robust tracking of the reference variable $i_q^*(t)$ (31), define the following sliding surface:

$$s_q(t) = i_q(t) - i_q^*(t) = 0 \tag{33}$$

where $i_q^*(t)$ is the reference variable for $i_q(t)$.

Theorem 3.2. *With reference to the system (18), (19) under Assumptions 2.1–3.1, the robust tracking of the reference current $i_q^*(t)$ is achieved after a finite time $t_q \geq t_f$ by a control law of the form:*

$$u_q(t) = u_q^{(eq)}(t) + u_q^{(n)}(t) \tag{34}$$

with:

$$u_q^{(eq)}(t) = Ri_q(t) \tag{35}$$

$$u_q^{(n)}(t) = -\left(\omega^M(L|i_d(t)| + \lambda_0) + L(\sigma + \eta_q)\right)\text{sign}(s_q(t)) \tag{36}$$

where $\sigma = \sup\left|\frac{di_q^*(t)}{dt}\right|$ according to (32), and $\eta_q > 0$ being an arbitrary positive constant.

Proof. The control law is designed imposing the condition ensuring the achievement of finite-time sliding motions (Utkin, Guldner, & Shi, 1999) on the surface (33), i.e. $s_q(t)\dot{s}_q(t) \leq -\eta_q|s_q(t)|$. After the insertion of (19) and (35), one has:

$$s_q(t)\left[u_q^{(n)}(t) + \omega(t)\left(\lambda_0 + Li_d(t)\right) - \frac{di_q^*(t)}{dt}\right] \leq -L\eta_q|s_q(t)| \tag{37}$$

and taking the worst case, the expression (36) immediately follows, ensuring that a sliding motion is established on the surface (33) (Utkin et al., 1999) after a finite time $t_q \geq t_f$ depending on the constant η_q. ■

With reference to the d-stator voltage, it can be easily determined imposing the attainment of a sliding motion on the surface

$$i_d(t) = 0. \tag{38}$$

The following lemma is given without proof.

Lemma 6. *With reference to the system (18), (19) under Assumptions 2.1–3.1, the robust tracking of the reference current $i_d(t) = 0$ is achieved after a finite time by a control law of the form:*

$$u_d(t) = u_d^{(eq)}(t) + u_d^{(n)}(t) \tag{39}$$

with:

$$u_d^{(eq)}(t) = Ri_d(t) \tag{40}$$

$$u_d^{(n)}(t) = -L\left(\omega^M|i_q(t)| + \eta_d\right)sign(i_d(t)) \tag{41}$$

$\eta_d > 0$ being an arbitrary positive constant.

The following corollary can finally be stated.

Corollary 7. *Define $i_q^*(t)$ as in (31). According to Theorem 3.2 the condition $i_q(t) = i_q^*(t)$ is robustly achieved after a finite time, i.e. the maximum energy conversion point is tracked in the presence of bounded parameter variations affecting the mechanical model. It follows that the robust achievement of the control objective $T_a(t) = T_{\text{opt}}(t)$ is guaranteed for bounded uncertainties affecting the WECS dynamical model, without any feedback coming from transducers measuring either wind speed, rotor position or rotor speed.*

4. Simulation tests

The proposed controller has been tested by intensive simulations using the model of the PMSG based WT given in the wind turbine control environment developed by Inc. Princeton Satellite Systems (2011). The simulated wind inflow consists of two components: the medium and long-term component associated to the macro-meteorological conditions (slower component) and the turbulence that covers the fast variations of the wind speed (short-term component). For the slower component the model is based on the discretization of the Van der Hoven spectrum and the model considered for the turbulence component is given by the von Karman power spectrum (Bianchi et al., 2007) (see Fig. 3). Note also that the wind mean value has been varied between 2 and 3 s.

Table 1
WECS parameter values (Inc. Princeton Satellite Systems, 2011).

WT parameters		
Rotor radius	m	$r = 3$
Rated wind speed	m/s	12.5
Rated rotational speed	rpm	310
PMSG parameters		
Winding resistance	ohm	$R = 4.3$
Winding inductance	mH	$L = 27$
Flux linkage	Wb	$\lambda_0 = 0.272$
Rated power	kW	20
Pole pairs	–	$N_r = 1$
Mechanical inertia	kg m^2	$J = 1$
Viscous friction	kg m^2/s	$K = 0.002$

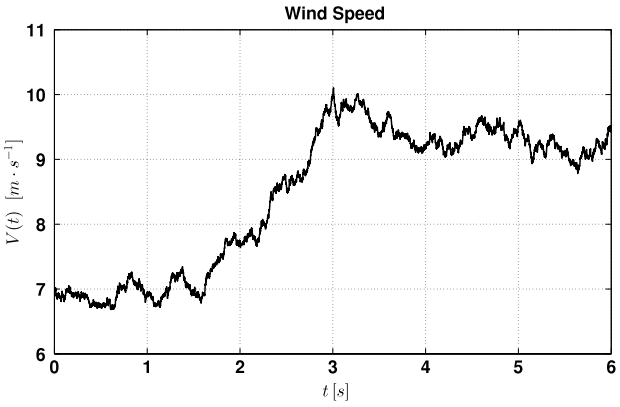

Fig. 3. Wind inflow.

The main parameters of the considered WECS are reported in Table 1. In all simulations, the sampling frequency has been selected as 0.1 kHz according to the real device specifications.

A 10% parameter variation has been considered to affect mechanical parameters J, B and K. Therefore: $\rho_J = 0.11$, $\rho_B = 1.1 \cdot 10^{-5}$, $\rho_K = 2.2 \cdot 10^{-4}$. Moreover, the following controller settings have been used: $\eta_\omega = 1$, $\eta_d = 1$, $\eta_q = 10$, $\gamma_\omega = 20$. Note also that boundary layers have been used to avoid chattering, replacing sign functions with saturation functions.

Some of the performed tests have been reported in Figs. 4(a)–8(b). Fig. 4(a) shows the aerodynamic torque, and Fig. 4(b) shows the torque error with respect to the optimal value. After a short transient, the torque error becomes significantly small, showing the effectiveness of the torque observer, which appears not to be influenced by wind variations.

Analogous considerations can be made for performances of the Rotor Position Derivation Subsystem and Rotor Speed Observer Subsystem. Fig. 5 shows the rotor angular position error, i.e. the variable $\theta_e(t) - \hat{\theta}_e(t)$, having denoted (13) by $\hat{\theta}_e(t)$. The rotor angular speed and the rotor angular speed observation error are depicted in Fig. 6(a) and (b), respectively.

The good performance achieved by the proposed solution in terms of efficiency of transferred energy is testified by results

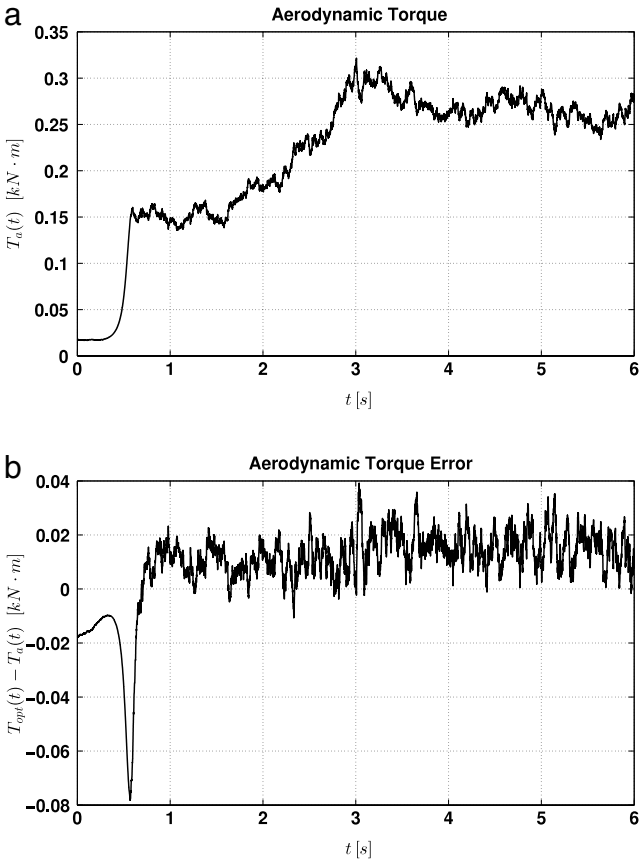

Fig. 4. (a) Aerodynamic torque; (b) Aerodynamic torque error.

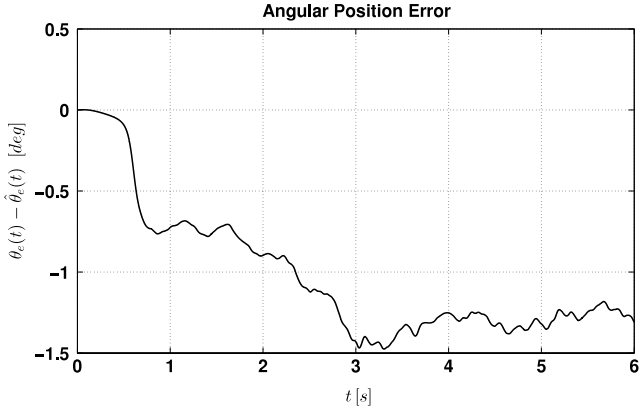

Fig. 5. Angular position error.

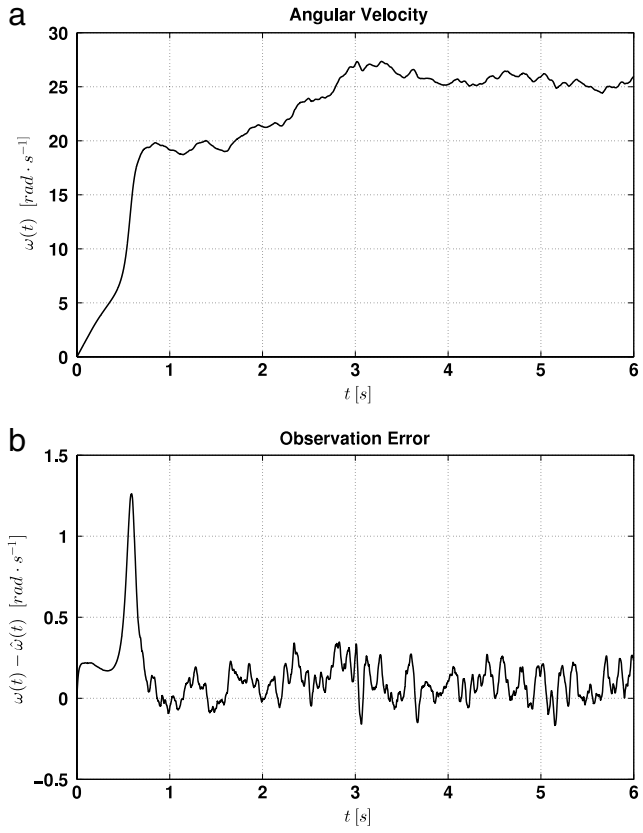

Fig. 6. (a) Rotor speed; (b) Rotor speed observation error.

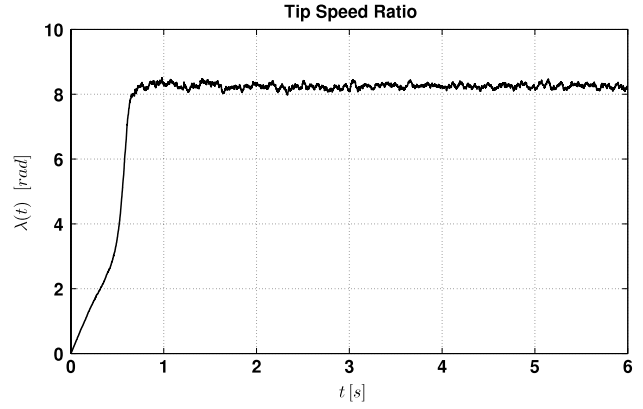

Fig. 7. Tip speed ratio.

reported in Fig. 7, showing that the tip speed ratio is maintained very close to its optimal value 8.1. Again, note that such behavior seems to be independent from wind mean value variations.

Finally, the practical feasibility of the proposed control system is shown in Fig. 8(a) and in Fig. 8(b), where the current $i_q(t)$ (Fig. 8(a)), and the voltage $u_q(t)$ (Fig. 8(b)) are reported. As is evident from these figures, the electrical variables are compatible with a possible practical implementation of the presented control architecture.

As a whole, simulations seem to prove the proposed sensorless observer-based control scheme behaves satisfactorily in the presence of parameter variations affecting the mechanical model parameters, and at the same time produces feasible control variables.

5. Conclusions

In this paper, a complete and novel robust sensorless control scheme has been proposed. The control policy has been shown able to ensure the achievement of maximum power efficiency of the WECS without feedback information about rotor speed and position, and about wind velocity. The proposed sensorless control strategy for WECS has been proved able to allow: the extraction of rotor position using electrical signals; the achievement of an exact estimate of the rotor speed within a finite time; the achievement of the condition on maximum power efficiency of the controlled WECS without the need of wind measurements and in the presence of bounded parameter variations affecting the mechanical system. An extensive simulation study has been reported to support the theoretical development.

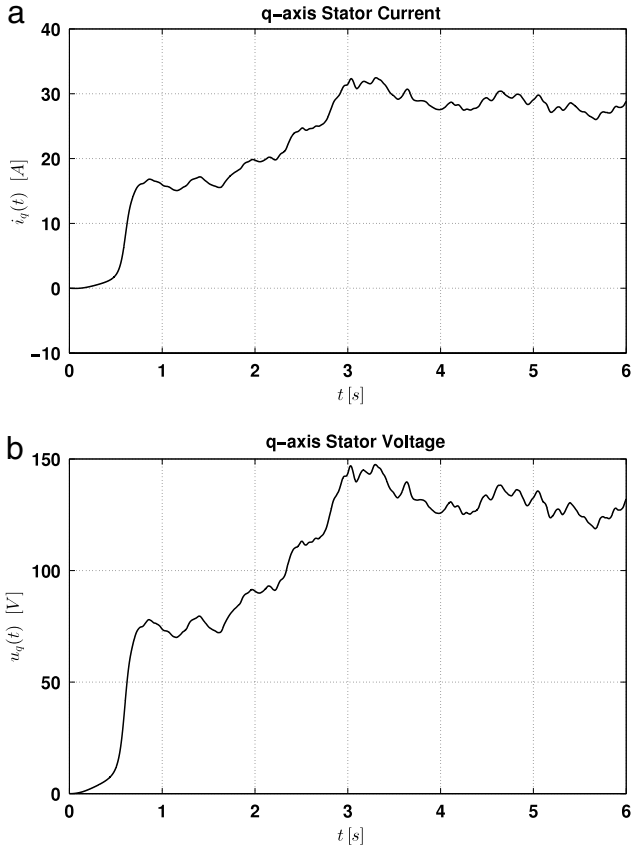

Fig. 8. Electrical variables: (a) Current $i_q(t)$; (b) Voltage $u_q(t)$.

References

Acarnley, P. P., & Watson, J. F. (2006). Review of position-sensorless operation of brushless permanent-magnet machines. *IEEE Transactions on Industrial Electronics*, *53*(2), 352–362.

Beltran, B., Ahmed-Ali, T., & Benbouzid, M. (2009). High-order sliding-mode control of variable-speed wind turbines. *IEEE Transactions on Industrial Electronics*, *56*(9), 3314–3321.

Bianchi, F. D., De Battista, H. N., & Mantz, R. J. (2007). *Wind turbine control systems: principles, modelling and gain scheduling design*. Berlin: Springer-Verlag.

Bolognani, S., Tubiana, L., & Zigliotto, M. (2003). Extended Kalman filter tuning in sensorless PMSM drives. *IEEE Transactions on Industry Applications*, *39*(6), 1741–1747.

Cadenas, Erasmo, & Rivera, Wilfrido (2009). Short term wind speed forecasting in La Venta, Oaxaca, Mexico, using artificial neural networks. *Renewable Energy*, *34*(1), 274–278.

Casadei, D., Profumo, F., Serra, G., & Tani, A. (2002). FOC and DTC: two viable schemes for induction motors torque control. *IEEE Transactions on Power Electronics*, *17*(5), 779–787.

Chen, Syuan-Yi, & Lin, Faa-Jeng (2011). Robust nonsingular terminal sliding-mode control for nonlinear magnetic bearing system. *IEEE Transactions on Control Systems Technology*, *19*(3), 636–643.

Chen, Z., Tomita, M., Doki, S., & Okuma, S. (2000). New adaptive sliding observers for position-and velocity-sensorless controls of brushless DC motors. *IEEE Transactions on Industrial Electronics*, *47*(3), 582–591.

Chinchilla, M., Arnaltes, S., & Burgos, J. C. (2006). Control of permanent-magnet generators applied to variable-speed wind-energy systems connected to the grid. *IEEE Transactions on Energy Conversion*, *21*(1), 130–135.

Corradini, M. L., Ippoliti, G., & Orlando, G. (2013). Robust control of variable-speed wind turbines based on an aerodynamic torque observer. *IEEE Transactions on Control Systems Technology 21*(4), 1199–1206.

El-Mokadem, M., Courtecuisse, V., Saudemont, C., Robyns, B., & Deuse, J. (2009). Experimental study of variable speed wind generator contribution to primary frequency control. *Renewable Energy*, *34*, 833–844.

Fernandez, R. D., Mantz, R. J., & Battaitotto, P. E. (2003). Sliding mode control for efficiency optimization of wind electrical pumping systems. *Wind Energy*, *6*, 161–178.

Ferreira, A., Bejarano, F. J., & Fridman, L. M. (2011). Robust control with exact uncertainties compensation: with or without chattering? *IEEE Transactions on Control Systems Technology*, *19*(5), 969–975.

Inc. Princeton Satellite Systems. (2011).

Johnson, K. E., Pao, L. Y., Balas, M. J., & Fingersh, L. J. (2006). Control of variable-speed wind turbines: standard and adaptive techniques for maximizing energy capture. *IEEE Control Systems Magazine*, *26*(3), 70–81.

Lee, J., Hong, J., Nam, K., Ortega, R., Praly, L., & Astolfi, A. (2010). Sensorless control of surface-mount permanent-magnet synchronous motors based on a nonlinear observer. *IEEE Transactions on Power Electronics*, *25*(2), 290–297.

Lee, Sung-Hun, Joo, Young-Jun, Back, J., & Seo, Jin Heon (2010). Sliding mode controller for torque and pitch control of wind power system based on PMSG. In *2010 Int. conf. contr. autom. sys.*, ICCAS (pp. 1079–1084).

Lopez, P., Velo, R., & Maseda, F. (2008). Effect of direction on wind speed estimation in complex terrain using neural networks. *Renewable Energy*, *33*(10), 2266–2272.

Mohamed, Y. A.-R. I. (2007). Design and implementation of a robust current-control scheme for a PMSM vector drive with a simple adaptive disturbance observer. *IEEE Transactions on Industrial Electronics*, *54*(4), 1981–1988.

Mohamed, Amal Z., Eskander, Mona N., & Ghali, Fadia A. (2001). Fuzzy logic control based maximum power tracking of a wind energy system. *Renewable Energy*, *23*(2), 235–245.

Monroy, A., & Alvarez-Icaza, L. (2006). Real-time identification of wind turbine rotor power coefficient. In *45th IEEE conf. dec. contr.* (pp. 3690–3695).

Murray, A., Palma, M., & Husain, A. (2008). Performance comparison of permanent magnet synchronous motors and controlled induction motors in washing machine applications using sensorless field oriented control. In *IEEE ind. appl. soc. annu. meet.*, IAS '08 (pp. 1–6).

Ortega, R., Praly, L., Astolfi, A., Lee, J., & Nam, K. (2011). Estimation of rotor position and speed of permanent magnet synchronous motors with guaranteed stability. *IEEE Transactions on Control Systems Technology*, *19*(3), 601–614.

Pahlevaninezhad, M., Eren, S., Bakhshai, A., & Jain, P. (2010). Maximum power point tracking of a wind energy conversion system using adaptive nonlinear approach. In *2010 annu. IEEE appl. pow. electron. conf.* (pp. 149–154).

Pao, L. Y., & Johnson, K. E. (2011). Control of wind turbines. *IEEE Control Systems Magazine*, *31*(2), 44–62.

Qiao, Wei, Qu, Liyan, & Harley, R. G. (2009). Control of IPM synchronous generator for maximum wind power generation considering magnetic saturation. *IEEE Transactions on Industry Applications*, *45*(3), 1095–1105.

Robles, E., Ceballos, S., Pou, J., Arias, A., Martin, J. L., & Ibanez, P. (2008). Permanent-magnet wind turbines control tuning and torque estimation improvements. In *15th IEEE int. conf. electron., circ. and sys., 2008*, ICECS 2008 (pp. 742–745).

Rossi, C., & Tonielli, A. (1994). Robust control of permanent magnet motors: VSS techniques lead to simple hardware implementations. *IEEE Transactions on Industrial Electronics*, *41*(4), 451–460.

Shyu, Kuo-Kai, Lai, Chiu-Keng, Tsai, Yao-Wen, & Yang, Ding-I (2002). A newly robust controller design for the position control of permanent-magnet synchronous motor. *IEEE Transactions on Industrial Electronics*, *49*(3), 558–565.

Siegfried, Heier (1998). *Grid integration of wind energy conversion systems*. John Wiley & Sons Ltd.

Tang, Choon Yik, Guo, Yi, & Jiang, J. N. (2011). Nonlinear dual-mode control of variable-speed wind turbines with doubly fed induction generators. *IEEE Transactions on Control Systems Technology*, *19*(4), 744–756.

Utkin, V., Guldner, J., & Shi, J. (1999). *Sliding mode control in electromechanical systems*. Florida, USA: CRC Press LLC.

Valenciaga, F., & Puleston, P. F. (2008). High-order sliding control for a wind energy conversion system based on a permanent magnet synchronous generator. *IEEE Transactions on Energy Conversion*, *23*(3), 860–867.

Wang, Baohua, & Qin, Shengsheng (2010). Backstepping sliding mode control of variable pitch wind power system. In *Pow. ener. eng. conf.*, APPEEC (pp. 1–3).

Xu, Zhuang, & Rahma, M. Faz (2007). Direct torque and flux regulation of an IPM synchronous motor drive using variable structure control approach. *IEEE Transactions on Power Electronics*, *22*(6), 2487–2498.

Yang, S. S., & Zhong, Y. S. (2007). Robust speed tracking of permanent magnet synchronous motor servo systems by equivalent disturbance attenuation. *IET Control Theory and Applications*, *1*(3), 595–603.

Zaragoza, Jordi, Pou, Josep, Arias, Antoni, Spiteri, Cyril, Robles, Eider, & Ceballos, Salvador (2011). Study and experimental verification of control tuning strategies in a variable speed wind energy conversion system. *Renewable Energy*, *36*(5), 1421–1430.

Zhong, L., Rahman, M. F., Hu, W. Y., Lim, K. W., & Rahman, M. A. (1999). A direct torque controller for permanent magnet synchronous motor drives. *IEEE Transactions on Energy Conversion*, *14*(3), 637–642.

Maria Letizia Corradini is currently serving as Full Professor of Automatic Control at the Scuola di Scienze e Tecnologie (Mathematics Division) of the University of Camerino. She received the Doctor's degree in Electronic Engineering from the University of Ancona and the Ph.D. degree from the University of Bologna in 1992. After having been employed by Honeywell Bull Italia, she was with the Dipartimento di Elettronica e Automatica of the University of Ancona as an Assistant Professor. She became Associate Professor of Automatic Control in 1998 at the University of Lecce, then Full Professor in 2001. She has published more than 150 papers on top rank international journals, books, and refereed conferences in the following areas: Variable Structure Control; Switching Control; Motors and Power devices; Robust Control in the presence of

non-smooth nonlinearities in actuators and sensors; Fault Tolerant Control, Modeling of Biological Systems; Mobile and Underwater Robotic. She is currently serving as Associate Editor of the IEEE Trans. on Automatic Control and of the IEEE Conference Editorial Board.

Gianluca Ippoliti received the Doctor's degree in electronic engineering and the Ph.D. degree in intelligent artificial systems from the Università Politecnica delle Marche (formerly University of Ancona), Ancona, Italy, in 1996 and 2002, respectively. From 1997 to 1998, he was with ISERM Unité 103, Montpellier, France and then with the University of Montpellier I, Montpellier, France, in the framework of the European research projects CAMARN and MOBINET. From 2002 to 2005, he was a Postdoctoral Fellow at the Dipartimento di Ingegneria Informatica, Gestionale e dell'Automazione, Università Politecnica delle Marche. Since March 2005, he is an Assistant Professor at the Università Politecnica delle Marche. His main research interests include switched systems and supervisory control, neural-network-based system identification and control, modeling identification and control of robotic, marine and electromechanical systems, and mobile robot control and localization.

Giuseppe Orlando was born in Isola del Liri (FR), Italy, on 12/07/1966, and lives in Osimo (AN). He received the Doctor's degree in electronic engineering and the Ph.D. degree in intelligent artificial systems from the Università Politecnica delle Marche, Ancona, Italy, in 1992 and 1996, respectively. From March 1994 to June 1994, he was visiting St. Louis Washington University, St. Louis, MO, with Prof. T.J. Tarn as Tutor. From 1997 to 2000, he was a Postdoctoral Fellow at the Dipartimento di Elettronica ed Automatica, Università Politecnica delle Marche. From October 2000 to October 2012, he was an Assistant Professor at the Università Politecnica delle Marche. Since November 2012, he is an Associate Professor at the same University. He is the author of about 90 scientific papers on international journals and conference proceedings. His main research interests include robust control, variable structure control, fault tolerant control, and control of marine systems.